RAVQ-HoloNet: Rate-Adaptive Vector-Quantized Hologram Compression

Shima Rafiei¹, Zahra Nabizadeh Shahr Babak¹, Shadrokh Samavi², and Shahram Shirani¹

¹McMaster University, Hamilton, Ontario, Canada ²Computer Science Department, Seattle University, Seattle, USA rafies1@mcmaster.ca

November 27, 2025

Abstract

Holography offers significant potential for AR/VR applications, yet its adoption is limited by the high demands of data compression. Existing deep learning approaches generally lack rate adaptivity within a single network. We present RAVQ-HoloNet, a rate-adaptive vector quantization framework that achieves high-fidelity reconstructions at low and ultralow bit rates, outperforming current state-of-the-art methods. In low bit, our method exceeds by -33.91% in BD-Rate and achieves a BD-PSNR of $1.02~\mathrm{dB}$ from the best existing method demonstrated by the rate-distortion curve.

1 Introduction

With the growing demand for immersive experiences in applications such as the metaverse, Augmented Reality (AR), and Virtual Reality (VR), holography has emerged as a key technology for generating realistic three-dimensional (3D) content. Holographic displays generate a three-dimensional scene by diffracting light through a hologram plane. The hologram plane serves as a medium that encodes interference patterns, capturing the light field corresponding to a three-dimensional scene. When illuminated, the hologram reconstructs the original wavefronts of the light. As these wavefronts reach the observer's eyes, they are perceived as if a real three-dimensional object, creating the illusion of a 3D scene [1]. The hologram, which preserves both the amplitude and phase information of the light field, can be created through optical setups or numerical simulation, known as Computer-Generated Holography (CGH). CGH enables the synthesis of holograms through numerical simulations or deep learning techniques, eliminating the need for complex optical setups. During the past decades, significant efforts have been devoted to developing methods for CGH.

1.1 Hologram Computation

Among computational approaches to CGH, traditional methods such as pointsource and wavefront propagation represent the object scene by its wave-emitting properties. Based on the Huygens-Fresnel principle, the point source method considers the object as a dense array of wave emitters, each radiating a spherical wavefront to construct the hologram via interference [2]. This approach, typically suited for point cloud objects, offers high reconstruction fidelity at the cost of significant computational complexity. Alternatively, layer-based methods use coherent planar wavefronts to efficiently model uniform surfaces, typically using Fresnel diffraction for near-field and the Angular Spectrum Method (ASM) for far-field scenarios [3]. This approach, typically suited for RGB-D and multilayer images. These methods commonly apply Fast Fourier Transforms (FFTs) to compute wave propagation efficiently via a propagator function in the frequency domain. Polygon-based approaches [4] further bridge the gap between complexity and efficiency by combining FFTs with coordinate transformations to handle diffraction from tilted surfaces. Despite their effectiveness, objectbased representation methods remain computationally demanding for large-scale or dynamic scenes. Recently, learning-based approaches have gained significant attention in CGH. For example, [5] proposed a CNN with focal stack loss that generates photorealistic, complex-valued 3D holograms in real time directly from polygonal mesh models reconstructed from captured point clouds.

In practical holographic display systems, Spatial Light Modulators (SLMs) are employed to modulate the wavefront of light for three-dimensional scene reconstruction. However, most commercially available SLMs are limited to phase-only modulation because of their higher diffraction efficiency and hardware simplicity [6].

When the complex-valued object wave is available, methods such as doublephase techniques [7, 8] or deep learning-based approaches [9, 10] are used to directly convert the complex field into a phase-only hologram. For instance, Double-Phase Amplitude Coding (DPAC) achieves this by mathematically decomposing the complex wavefront into two phase-only components with constant amplitude, facilitating accurate reconstruction without iterative computation. [5] proposed an Anti-Aliasing Double-Phase method (AA-DPM), a modified DPAC approach designed specifically for CNN-predicted complex holograms, which effectively mitigates aliasing artifacts around high-frequency details and occlusion boundaries. Other methods, such as direct deep learning methods, aim to predict phase-only holograms, typically in an unsupervised manner. These approaches typically employ an encoder-decoder architecture trained to map intensity distributions into phase-only holograms. Recent models include HoloNet [9], DeepCGH [10], DGH [11], and 3D-DGH [12] as unsupervised methods. The method proposed in [6] employs supervised learning followed by unsupervised learning. In unsupervised settings [9, 10], CNNs are trained to generate phase-only holograms using only the target intensity (amplitude) at one or more depth planes as supervision. Without access to the ground-truth phase, the network autonomously learns to produce the appropriate phase-only hologram that reconstructs the desired intensity. It is analogous to traditional optimization-based approaches such as Stochastic gradient descent (SGD) or the Gerchberg–Saxton (GS) method as phase retrieval algorithms [13], where the complex object wave is unknown, and a randomly initialized phase is iteratively updated—either through gradient backpropagation in the case of SGD-based methods or through alternating projections in the GS algorithm—to reconstruct a phase pattern that yields the desired target intensity upon propagation.

Recent studies [9] have shown that stochastic gradient descent (SGD) outperforms classical methods such as DPAC, as well as deep-learning-based approaches like HOLONET, but it is highly time-intensive, requiring many iterations to achieve enhancement [9, 6].

1.2 Hologram Compression

To enable low-power real-time holographic applications, hologram compression is essential to reduce storage, transmission, and processing costs [14] along with optimized computational pipelines, especially for VR/AR near-eye holographic displays [15]. [8] demonstrated the feasibility of AR/VR systems by shifting optical complexity to software through Fresnel holography to synthesize object wavefronts, allowing for improved control over most of the system constraints.

However, as holography advances toward practical deployment in AR/VR, it paves the way for real-time applications and interactive entertainment, where low latency and high visual fidelity are essential [15].

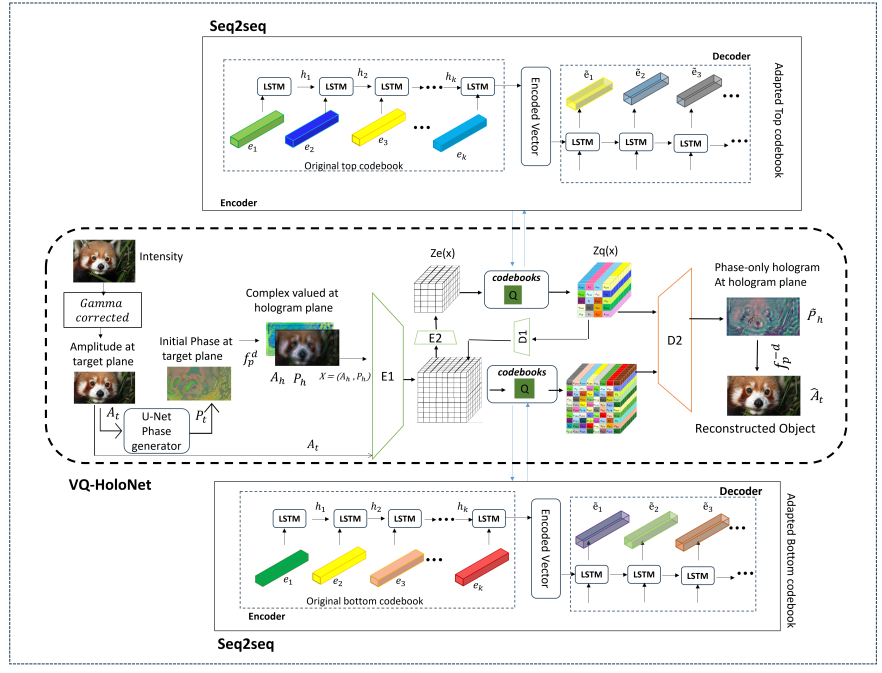
Despite the growing interest in holographic displays, limited research methods have focused specifically on hologram compression. [15] introduced a unified framework that integrates hologram generation and compression, in which the computationally intensive hologram generation is offloaded to a sender, such as a cloud server (encoder). A lightweight decoding is performed on a receiver edge device. By transmitting a compact latent representation, the method enables fast and efficient data transfer. Other methods typically treat hologram computation and compression as separate steps. One common approach is first to compute the hologram and then apply standard image or video codecs for compression. However, traditional codecs such as JPEG, HEVC, and H.264 are ill-suited for holographic content. The high-frequency interference patterns and phase-dependent details intrinsic to holograms often lead to significant quality degradation when compressed using these general-purpose standards [16]. Hence, learning-based methods have shown greater success. [17] introduces a deep learning framework for phase-only hologram based on [18]. By employing a phase-specific distortion metric and entropy bottleneck, the method outperforms traditional codecs such as VVC in rate-distortion performance on the non-public ETRI dataset. [19] also proposes a hybrid approach for holographic complex-valued video compression, combining H.265 video coding with the Hi-FiHC neural network as a conditional Generative Adversarial Network (GAN). Motion vectors are used to predict inter-frame content, while a deep neural network encodes the residual errors to capture fine holographic details, enabling efficient compression of temporally coherent holographic sequences. The latent space of the network is compressed based on the Ballé method. [20] changed [15] by dividing holographic content into distinct foveated and peripheral areas. It applies higher compression to peripheral areas, where human vision is less sensitive, while preserving high-quality in the foveated region. While recent neural compression methods for holograms have shown promising results, most are fundamentally based on the Ballé-style framework, utilizing continuous latent variables, hyperprior models, and entropy bottlenecks for compression [17, 15, 19, 20]. These approaches follow the rate-distortion optimization principles laid out in [21, 18], adapting them to holographic data. In contrast, our method departs from this convention by employing a VQ-VAE based approach, which learns a discrete latent space more suited for complex-valued holograms and offers superior performance in bit-per-pixel (Bpp) and PSNR. To the best of our knowledge, no prior work has applied vector quantization in the latent, or feature domain, to compress phase or complex holograms, making our approach both novel and well-aligned with the demands of real-time AR/VR systems. In this paper, we propose a pipeline of joint hologram computation and compression in an unsupervised manner similar to HoloNet [9], aiming to generate phase-only holograms with built-in compression inspired by [22]. During training, we employ the ASM for wave propagation. However, learned propagators such as those proposed in [9] can be integrated to model hardware-specific aberration-corrected phase-only holograms. We proposed a VAE-inspired architecture for end-to-end optimized hologram compression. Main contributions are as follows:

- We propose an unsupervised hologram compression based on a hierarchical VQ-HoloNet architecture, which learns discrete latent representations without ground-truth phase supervision.
- The model is rate-adaptive through its multi-level vector quantization structure, enabling control over compression rate and reconstruction quality.
- Our hologram compressor accepts either complex holograms or intensityonly inputs and compresses them, subsequently decompressing the data into phase-only holograms. Therefore, the proposed method can operate as either a hologram generator-compressor or a standalone compressor, depending on the type of input provided.

The paper is structured as follows: Section 2 presents the proposed method, including its architecture and the loss functions used. Section 3 describes the implementation and analyzes the results. Finally, the conclusion summarizes our work.

2 Proposed Method

Holographic data inherently requires significant storage and transmission bandwidth. Efficient compression is therefore critical for enabling real-time holo-



RAVQ-HoloNet

Figure 1: The block diagram of the proposed method. Illustration of the codebook adaptation framework. The process begins with the original codebook $\mathbf{e} = \{e_1, e_2, \dots, e_K\}$. These are passed through a Seq2seq model composed of LSTM units to produce an intermediate representation. A subsequent decoder transforms this representation into the adapted codebook $\tilde{\mathbf{e}} = \{\tilde{e}_1, \tilde{e}_2, \dots, \tilde{e}_K\}$, illustrated for the top and bottom codebooks.

graphic applications, especially on resource-constrained edge devices. Our proposed unsupervised framework integrates two key components: (1) an initial (optional) complex hologram generation stage based on a U-Net. This stage can be bypassed if a complex hologram is available rather than the object intensity, and (2) hologram compression via a Rate Adaptive Vector Quantized HoloNet (RAVQ-HoloNet), where a central contribution of our approach is the unification of the complex-valued encoder and the phase-only hologram decoder within a single network. As shown in Fig. 1, our RAVQ-HoloNet model, consists of VQ-HoloNet, depicted in the middle box, and two sequence-to-sequence (Seq2seq) models on the top and the bottom. In the VQ-HoloNet part, the encoder operates directly on the input complex-valued hologram and extracts features from this complex input. The subsequent part of the decoder then processes these features to generate the phase-only hologram.

Inspired by the VQ-VAE-2 architecture [23], VQ-HoloNet is composed of three main components: a complex-valued encoder, a vector quantization module, and a lightweight decoder that generates the final phase-only holograms. In conventional VQ-VAE models, the vector quantization component lacks flexibility in adjusting compression levels and typically requires retraining for each desired bitrate or compression ratio. This approach results in needing separate networks for each compression setting, which demands extra storage to maintain multiple encoders on the sender side and corresponding decoders on the receiver side—an impractical solution for edge devices with limited storage capacity. To overcome this limitation, we incorporate Seq2seq models, as originally introduced in [22], to compress the codebooks produced by our VQ-HoloNet at multiple bitrates. This enables rate-adaptive compression and completes the RAVQ-HoloNet architecture. The block diagram of the proposed framework is shown in Fig. 1. The details of each component are described in the following sections.

2.1 Complex Hologram Generation

In the first stage of our proposed framework, an intensity image serves as the input. This image is initially transformed into a target amplitude (A_t) by applying the inverse of Gamma correction, followed by a square root operation, as described in [9]. The inverse Gamma correction is used to counteract the Gamma adjustment performed by the camera. The resulting amplitude is then used to generate an initial phase estimate (P_t) using a pre-trained U-Net from [15]. These two components—the target amplitude and the generated phase—are combined to form a complex-valued light field in the object domain (target plane). This complex field is subsequently propagated to the hologram plane using a bandwidth-limited ASM with a propagation distance of d. The propagated field provides both the amplitude (A_h) and phase (P_h) at the hologram plane.

Because ASM introduces numerical errors and constrains reconstruction accuracy [3], we address this challenge by providing our RAVQ-HoloNet with both the complex-valued hologram from the hologram plane and the target amplitude from the object domain. This approach enables the network to decode a more accurate phase-only output, resulting in improved reconstruction of the desired intensity in the object domain.

The mathematical formulation of the ASM, which is used to simulate wave propagation, will be presented in the loss function section, as it is essential for computing the reconstruction loss in the object domain.

2.2 Hologram Compression

In the compression stage of our framework, the hologram is encoded into a compact representation referred to as the *latent space*, which contains all the information required for subsequent reconstruction. To achieve this, we propose an encoder-decoder-based architecture, VQ-HoloNet, which is specifically designed to compress complex-valued holographic data and reconstruct phase-only output. VQ-HoloNet employs two hierarchically organized, multi-scale encoders,

 E_1 and E_2 , together with their respective decoders, D_1 and D_2 . Each encoder-decoder pair is constructed from R residual blocks, allowing the model to effectively capture both coarse and fine features present in the hologram. Hierarchical latent representations are widely used in state-of-the-art image compression frameworks for natural images [23], as they enable the model to simultaneously capture global structures and local details, leading to high-fidelity reconstructions. In our work, to make the compressed representation suitable for efficient storage and transmission, it is necessary to map the continuous latent space to a discrete space. For this purpose, we employ vector quantization.

Vector quantization is particularly well-suited to holographic data, as previous studies [24] have shown that holograms exhibit low histogram variation compared to natural images. These properties result in statistical redundancy in complex wavefronts, making vector quantization an effective choice for compression.

To perform quantization, we utilize the Exponential Moving Average (EMA) clustering algorithm [25]. This algorithm assigns each latent vector to the nearest entry in a learnable codebook, where each codebook entry acts as the centroid of a cluster. During training, the codebook is continuously updated to represent the most salient features in the data.

The hierarchical structure operates as follows (see Fig. 1): The top-level latent representation is first quantized and decoded. This decoded representation is then concatenated with the bottom-level latent before it is quantized. The combined latent is quantized and merged with the upsampled, quantized top latent for joint decoding. This hierarchical process allows the model to capture both high-level and detailed information in the hologram. To achieve different compression rates for the discrete latent codebooks and enable adaptive rate control, we integrate the VQ-HoloNet structure with an embedded Seq2seq encoder-decoder, as originally proposed in [22]. This addition allows the codebooks generated by VQ-HoloNet to be further compressed at multiple bitrates, making the overall framework both flexible and efficient. In summary, this compression stage provides an end-to-end solution for hologram compression, leveraging hierarchical latent representations, vector quantization, and rate-adaptive codebook compression.

2.2.1 Rate-Adaptive Seq2seq Model

Achieving different compression ratios in our framework is largely influenced by the number of codebook entries. To enable flexible bitrate control, we integrate a Seq2seq encoder-decoder model that can adaptively adjust the codebook size, effectively transforming the codebook from size A to size B as needed. This integration allows our framework to incorporate a bitrate tuner directly within a single network, enabling dynamic and real-time adjustment of the compression ratio during inference.

Unlike Ballé-based compression networks, which require training and storing separate model weights for each compression level, our method supports a continuous spectrum of bitrate-quality trade-offs using the same model. This

flexibility makes our approach especially suitable for adaptive compression scenarios, such as real-time quality-of-service (QoS) management over variable network conditions. The adapted codebook, denoted as $\tilde{\mathbf{e}} = \{\tilde{e}_1, \tilde{e}_2, \dots, \tilde{e}_k\}$, is generated by the Seq2seq model, which utilizes a series of Long Short-Term Memory (LSTM) [26, 27] units to sequentially encode and decode the code vectors. In this context, codebook entries are treated analogously to words in a sentence, allowing the LSTM encoder to summarize the original codebook and the LSTM decoder to reconstruct a compact codebook of the desired size. The target codebook size, $K_{\tilde{e}}$, can be specified by the user or dynamically selected based on network requirements.

During training, our RAVQ-HoloNet is optimized using various codebook sizes to ensure robustness and adaptability. At inference time, the Seq2seq model dynamically generates the adapted codebook $\tilde{\mathbf{e}}$, thereby matching the output bitrate to the current application demands.

2.3 Communication

The hologram is compressed on the sender side and decompressed on the receiver side for use. Fig. 2 illustrates the process of data transfer from the sender to the receiver, which could be an edge client [15].

As shown in the figure, only codebooks of various sizes are pre-stored on both the sender and receiver sides, eliminating the need to regenerate them with the Seq2seq model for each transmission. In other words, after training, codebooks of different sizes can be generated using the Seq2seq model and subsequently stored on both ends. The same VQ-HoloNet encoder is used on the sender side, and the same decoder on the receiver side, regardless of the codebook size. This strategy significantly reduces transmission time and removes the requirement for the Seq2seq model during inference. When an image is input to the network, it is first encoded into continuous latent feature maps. These latent maps are then quantized by mapping each one to the nearest discrete vector in the selected codebook. The choice of codebook depends on the network's Quality of Service (QoS) requirements; typically, higher-quality service employs larger codebooks. Since the necessary codebooks are already stored at the receiver side, only the sequence of corresponding indices needs to be transmitted, instead of the full quantized feature vectors [25]. This is highly advantageous, as quantized feature vectors are high-dimensional (e.g., 128 dimensions) and stored with floatingpoint precision, resulting in much greater transmission costs than the integer indices. To further enhance compression efficiency, the indices are entropy-coded using Huffman coding [28], as depicted in Fig. 2.

2.4 Training and Loss Functions

We train our model in two stages. In the first stage, we disable the Seq2seq unit and train the base model. After the base model is trained for W epochs, we activate the Seq2seq. In the first stage, we use the following loss:

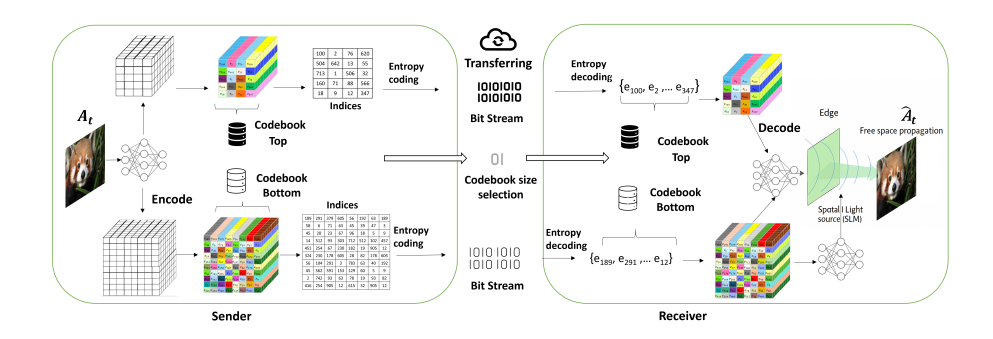


Figure 2: A simplified illustration of the sender-receiver hologram communication framework.

$$\mathcal{L}_{\text{framework}} = \text{Latent}_{\text{VQ}}(\mathbf{e}) + \mathcal{L}_{\text{VQ}_{\text{Beconstruct}}}(\mathbf{e}) \tag{1}$$

The complex hologram $\mathbf{x} = (A_h, P_h)$ is encoded into a latent representation by the encoder and then quantized using a learned codebook; the quantizer maps each encoder output to its nearest codebook vector:

$$z_q(\mathbf{x}) = Q(E_{\theta}(\mathbf{x})|\mathbf{e}) = \arg\min_{0 \le i \le K} ||E_{\theta}(\mathbf{x}) - e_i||_2$$
 (2)

where $z_q(\mathbf{x})$ is the quantized latent, and E_{θ} is the encoder. The decoder D_{ϕ} reconstructs the phase-only hologram:

$$\tilde{P}_h = D_\phi(z_q(\mathbf{x})) \tag{3}$$

Because the codebook is learned during training, we add a dedicated loss to regulate it. Since quantization is non-differentiable, so we adopt the straight-through estimator to backpropagate gradients. The overall objective therefore includes two components: a codebook loss and a commitment loss.

$$\operatorname{Latent_{VQ}}(\mathbf{e}) = \underbrace{\|\operatorname{sg}[E_{\theta}(\mathbf{x})] - z_{q}(\mathbf{x})\|_{2}^{2}}_{\operatorname{Codebook\ Loss}} + \beta \underbrace{\|\operatorname{sg}[z_{q}(\mathbf{x})] - E_{\theta}(\mathbf{x})\|_{2}^{2}}_{\operatorname{Commitment\ Loss}}$$

$$(4)$$

where $sg[\cdot]$ denotes the stop-gradient operation, and β is a hyperparameter.

As shown in Eq. 1, this stage also has a reconstruction loss $\mathcal{L}_{VQ_{Reconstruct}(\mathbf{e})}$. Due to the high-frequency phase variations in holographic data, neural networks may struggle to learn accurate phase reconstructions. To address this, we incorporate a physics-inspired wave propagation model into our loss function, guiding the network with a differentiable forward model that simulates light propagation. While the Rayleigh–Sommerfeld (RS) integral [29, 2] is the most accurate,

it is computationally expensive. For efficiency, we use the band-limited ASM [3], formulated as:

$$f_p^d(\phi, a) = \iint \mathcal{F}\left[e^{i\phi(x,y)}a(x,y)\right] \cdot H(f_x, f_y, d) \cdot e^{i2\pi(f_x x + f_y y)} df_x df_y,$$
(5)

where \mathcal{F} denotes the 2D Fourier transform, f_x and f_y are spatial frequencies, a(x,y) is the amplitude, and $H(f_x, f_y, d)$ is the kernel function:

$$H(f_x, f_y, d) = \begin{cases} \exp\left(i\frac{2\pi d}{\lambda}\sqrt{1 - (\lambda f_x)^2 - (\lambda f_y)^2}\right), & \text{if } f_x^2 + f_y^2 < \frac{1}{\lambda^2}, \\ 0, & \text{otherwise.} \end{cases}$$
(6)

 $\phi(x,y)$ is a real-valued discrete phase map, and $H(f_x,f_y)$ acts as a low-pass filter, removing spatial frequencies beyond the physical cutoff defined by the wavelength λ . The forward model $f_p^d(\phi,a)$ numerically propagates the complex field from the hologram to the target plane. While the inverse hologram propagation to the object domain enables us to compare the reconstructed amplitude $|\hat{A}_t| = |f_p^{-d}(\phi,1)|$ with the ground truth amplitude A_t .

For computational efficiency, ASM is expressed in the Fourier domain:

$$f_p^d(\phi, a) = \mathcal{F}^{-1} \left\{ \mathcal{F} \left[a(x, y) e^{i\phi(x, y)} \right] \cdot H(f_x, f_y, d) \right\},$$

where \mathcal{F}^{-1} is the inverse 2D Fourier transform.

To ensure high-quality phase retrieval, we combine three complementary loss terms between the reconstructed amplitude $|\hat{A}_t| = |f_p^{-d}(\phi, 1)|$ and the target amplitude A_t :

- MSE Loss: Pixel-wise mean squared error.
- MS-SSIM: Multi-Scale Structural Similarity Index for perceptual quality [30].
- Watson-DFT: Frequency-domain perceptual loss [31].

The reconstruction loss is:

$$\mathcal{L}_{\text{VQ}_{\text{Reconstruct}}(\mathbf{e})} = a_{\text{MSE}} \cdot \mathcal{L}_{\text{MSE}} + a_{\text{MS-SSIM}} \cdot (1 - \mathcal{L}_{\text{MS-SSIM}}) + a_{\text{WFFT}} \cdot \mathcal{L}_{\text{WFFT}}, (7)$$

where $a_{\text{MSE}}, a_{\text{MS-SSIM}}, a_{\text{WFFT}}$ are weighting coefficients. In fact, to calculate $\mathcal{L}_{\text{VQ}_{\text{Reconstruct}}}$, the phase-only map is first reconstructed to the object domain using ASM in Eq. 5, then quality metrics are applied between the reconstructed object and the original amplitude.

In the second stage, the Seq2seq is activated after training the first stage for W epochs. By activating Seq2seq, the generated codebook is fed to Seq2seq, and a new codebook would be generated. So the framework loss would be changed as follow:

$$\mathcal{L}_{\mathrm{framework}} = \mathrm{Latent}_{\mathrm{VQ}}(\tilde{\mathbf{e}}) + \mathcal{L}_{\mathrm{VQ}_{\mathrm{Reconstruct}}}(\tilde{\mathbf{e}}) \tag{8}$$

where $\tilde{\mathbf{e}}$ is the output of the Seq2seq. Gradients in the Seq2seq model are backpropagated through the decoder and latent space toward both the LSTM encoder and decoder, enabling the model to adapt to varying codebook sizes. For newly introduced codebook sizes, the objective is to achieve low latent loss while maintaining high reconstruction quality.

3 Experimental Results

This section first provides an overview of the dataset and the optical setup used in our experiments. We then describe the network configuration in detail, followed by a comprehensive presentation of both quantitative and qualitative analyses of our results. The effectiveness of the proposed method is demonstrated and discussed based on various performance metrics and visual comparisons.

3.1 Dataset

To fairly evaluate and compare the performance of different compression methods, a public dataset with consistent simulated optical parameters is essential. In our experiments, we utilize the DIV2K dataset [32], which comprises 800 images and is commonly used for compression evaluation purposes. For testing, we adopt a distinct set: a 100-image validation subset from [15].

In our experiments, the pixel pitch of the hologram plane was set to $6.4\,\mu\mathrm{m}$. RGB illumination was employed, using wavelengths of $450\,\mathrm{nm}$ (blue), $520\,\mathrm{nm}$ (green), and $638\,\mathrm{nm}$ (red). The propagation distance between the object plane and the hologram plane was fixed at $20\,\mathrm{cm}$. Due to the wavelength-dependent nature of diffraction, a separate model was trained for each color channel.

3.2 Development Platform

The proposed method was implemented on a platform equipped with an RTX 4090 GPU (24 GB VRAM) and a 13th Gen Intel(R) Core(TM) i9-13900 CPU.

3.3 Previous Work

Several previous methods have addressed the challenge of hologram compression. [15, 20, 17, 19] follow the approach proposed by Ballé et al. [18], which handles the non-differentiability of quantization by replacing it with a differentiable approximation. This is achieved by adding uniform noise during training and employing a learned prior for entropy modeling. Such techniques enable end-to-end optimization based on the rate-distortion objective, allowing the trade-off between bitrate and reconstruction quality to be controlled by adjusting the distortion weight. Typically, these methods require separate models or network weights to operate at different target bitrates (e.g., low, medium, high). While Ballé-based methods offer a practical workaround for quantization non-differentiability, they have some limitations. They often require training and

maintaining multiple models to support different bitrates, making them less efficient for adaptive compression tasks. In contrast, our proposed VQ-HoloNet introduces a built-in bitrate tuner that enables dynamic control over the compression ratio within a single unified network. This flexibility allows the model to adjust the bitrate on demand—without the need for retraining or uploading additional weights—making it particularly well-suited for adaptive compression scenarios, such as quality-of-service (QoS) control over networks. Additionally, [20] uses a multi-network architecture, employing two U-Nets—one as a phase initializer and the other as a phase generator. This design increases the computational burden on head-mounted hardware, as an additional phase generator is needed after the decompression. Our method, on the other hand, reduces this computational load by integrating the necessary functionality into a more efficient, single-network design.

3.4 Compression Viewpoint

In this work, we approach compression from two perspectives within our model architecture.

- 1) Reducing the number of code vectors in the dictionary. By decreasing the number of available code vectors, the number of bits required to store the code vectors' indices is reduced. To enable this flexibility, a Seq2seq module is integrated into the network to generate varying numbers of code vectors. During training, the VQ-HoloNet backbone is first trained for W=100 epochs. After this warm-up phase, the Seq2seq component is activated. This staged training strategy improves codebook utilization by allowing the encoder to learn robust representations before the network becomes rate-adaptive. We refer to this configuration as the low model. In this model, the latent representations have spatial resolutions of 268×480 for the bottom level and 134×240 for the top level.
- 2) Reducing the number of latent features to be transmitted. In the second approach, compression is achieved by reducing the number of feature maps in the latent space. This is implemented by decreasing the number of filters in the convolutional layers compared to the low-bitrate model. By lowering the latent features dimensionality, width and height, a lower effective bitrate can be achieved. We refer to this configuration as the *ultra-low model*. In this approach, the model has the same architecture with deeper layers having an extra downsampling step to half the spatial resolution at each level: 134×240 for the bottom level and 67×120 for the top level.

Both approaches can be combined or tuned independently to achieve the desired trade-off between bitrate and reconstruction quality, enabling flexible adaptation to bandwidth constraints while preserving visual fidelity as much as possible.

3.5 Network Configuration

The encoder and decoder in the phase generation module of VQ-HoloNet are constructed using an initial series of deformable convolutional layers [33, 34]. Normal convolutions sample features on a fixed grid, limiting their ability to capture irregular fringes and distortions in phase maps. Experimentally, this results in more accurate phase generation and improved efficiency compared to standard convolutions. Deformable convolutions introduce learnable offsets, enabling adaptive receptive fields that align with local phase variations. In the encoder, the deformable convolutions are followed by R=4 residual blocks, each with a residual channel depth of 128. We set the reconstruction loss weights as $w_{\rm MSE}=1,~w_{\rm MS-SSIM}=0.1,$ and $w_{\rm WFFT}=0.025$ to balance pixel-wise accuracy, perceptual similarity, and frequency-domain fidelity. The decoder utilizes transposed convolutions for upsampling. Each residual block contains one deformable convolution and one standard 1×1 convolution as well, similarly with a residual channel depth of 128.

The latent space is represented by a codebook. This codebook comprises 4096 discrete embeddings (code vectors), each represented by a 128-dimensional vector. The Seq2seq model is trained to operate over a continuous range of embedding counts, allowing $K_{\tilde{e}}$ to be any value between 512 and 4096 to allow compression at different bit rates. However, during inference, the model is constrained to generate codebooks whose sizes are powers of two (i.e., $K_{\tilde{e}} = 512, 1024, 2048, \text{ or } 4096$). Although entropy coding methods such as Huffman coding can support arbitrary codebook sizes, adhering to powers of two simplifies hardware implementation and maintains consistency with standard quantization practices.

In our implementation, the EMA decay for codebook updates is set to 0.95, and the commitment cost is fixed at 0.25. Furthermore, the network is optimized using the Adam optimizer with a constant learning rate of $\eta=1\times 10^{-4}$. The original image size is 1072×1920 . To reduce ringing artifacts after ASM propagation, we set the region of interest (ROI) to 700×1400 and apply additional zero padding for stability, following the approach in [20].

3.6 Quantitative Results

Table 1 compares the performance of three models—VQ-HoloNet Low, VQ-HoloNet Ultra-Low, and Dual Phase Retrieval and Compression (DPRC) [15]—in terms of reconstruction quality and compression efficiency. Both VQ-HoloNet Low and VQ-HoloNet Ultra-Low achieve comparable or slightly reduced perceptual quality relative to the DPRC-High Quality model, while operating at significantly lower Bpp rates. VQ-HoloNet Low attains a PSNR of 29.43 dB at a Bpp of 1.787, whereas DPRC requires 3.5 Bpp (approximately 2 times compare to our low model) to achieve a similar quality. VQ-HoloNet Ultra-Low further reduces the Bpp by approximately 78% compared to the Low model, while only decreasing the PSNR by about 13%. As shown in Fig. 3, VQ-HoloNet-Low preserves quality despite using fewer Bpp. These results demonstrate the effec-

Table 1: Quantitative comparison of reconstruction quality and compression efficiency across three channels.

Method	↑ PSNR	† SSIM	↓ LPIPS	$\overline{\mathbf{S}\downarrow\mathbf{Bpp}}$
VQ-HoloNet Low	29.43	0.84	0.25	1.787
VQ-HoloNet Ultera Low	26.00	0.7	0.4	0.4
DPRC-High Quality	29.67	0.87	0.2	3.50







(a) Original image

(b) DPRC High Quality

(c) VQ-HoloNet Low

Figure 3: A quantitative result of VQ-HoloNet vs. DPRC

tiveness of our quantization strategy in the VQ-HoloNet models, which maintain high visual fidelity even at substantially reduced bitrates—unlike DPRC, which depends on high-quality quantization and a larger latent space to achieve optimal reconstruction quality.

With VQ-HoloNet Low, our method achieves significantly lower Bpp values while maintaining quality close to the DPRC-High Quality model, which relies on a larger latent space and higher quantization for optimal fidelity. Table 2 shows the size of the latent space based on H and W, the size of the input, before VQ quantization, in float, and after VQ quantization, in bits. However, our VQ-HoloNet does not fully utilize the entire 4096-entry codebook (12-bit representation). Codebook utilization denotes the fraction of code vectors that are selected at least once to encode features within a dataset. Fig. 5(d) illustrates the probability distribution of code vector utilization for both the Top and Bottom layers across all channels in the test set. A higher utilization percentage indicates broader coverage of the codebook, whereas a lower utilization reflects reliance on a smaller subset of code vectors, which can reduce the Bpp rate but may also degrade reconstruction quality. As shown, the Bottom layer exhibits a more skewed distribution compared to the Top layer. This indicates relatively higher utilization, which can have a significant impact on the quality of reconstruction. The Top codebook exhibits lower utilization, as it encodes

Table 2: Quantitative comparison of latent space and the quantization.

Method	Latent Spaces (float)	Quantized (bit)
VQ-HoloNet Low	$128 \times \left(\frac{H}{4} \times \frac{W}{4} + \frac{H}{8} \times \frac{W}{8}\right)$	$12 \times \left(\frac{H}{4} \times \frac{W}{4} + \frac{H}{8} \times \frac{W}{8}\right)$
VQ-HoloNet Ultera Low	$128 \times \left(\frac{H}{8} \times \frac{W}{8} + \frac{H}{16} \times \frac{W}{16}\right)$	$12 \times \left(\frac{H}{8} \times \frac{W}{8} + \frac{H}{16} \times \frac{W}{16}\right)$

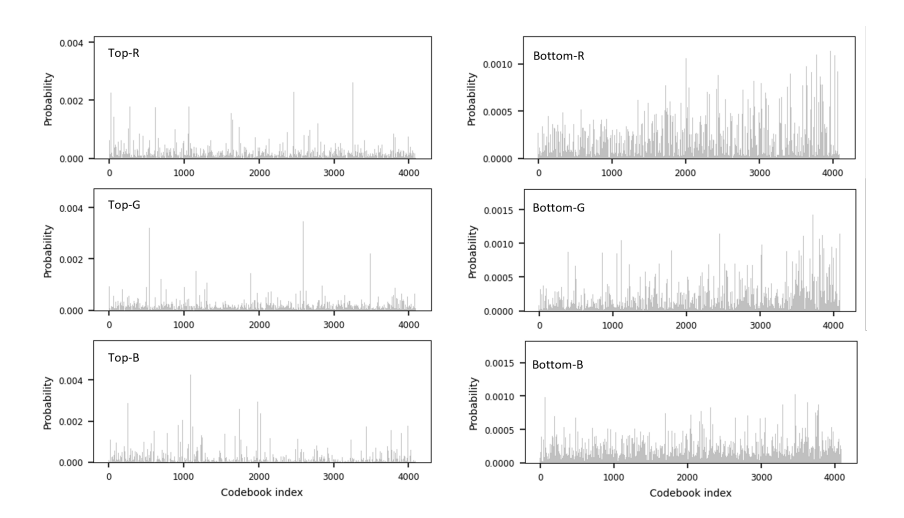


Figure 4: Probability of codebook indices selected in each layer of the Bottom and Top across the test set, for each channel.

more abstract and high-level features that require fewer distinct embeddings. In contrast, the Bottom layer achieves approximately 90% utilization, indicating relatively high codebook usage for representing phase-only holograms. Fig. 4 illustrates the frequency of each code vector across test images for each channel. As shown, both the Top and Bottom layers of each channel exhibit non-uniform code vector selection, where some code vectors occur far more frequently than others. This imbalance in code vector distribution highlights the potential of entropy coding to further improve compression efficiency. Representing these indices requires 12 bits (0.75 Bpp) for the bottom and 12 bits (0.187 Bpp) per channel for the top. In total, before entropy coding, the bitrate is 0.937 Bpp for each channel, which is reduced to 0.6 Bpp per channels B and R and 0.59 Bpp per G channel after Huffman coding. Fig. 5 presents the rate-distortion performance of our proposed method compared to several existing techniques, evaluated using PSNR, SSIM [35], and LPIPS [36] metrics. Results are plotted against bits per pixel (Bpp) to illustrate the trade-off between compression rate and visual quality. Our approach is tested under two compression modes: "Low" and "Ultra Low". Even at very low bitrates, our method maintains competitive or superior visual quality, as indicated by higher PSNR and SSIM values and lower LPIPS scores.

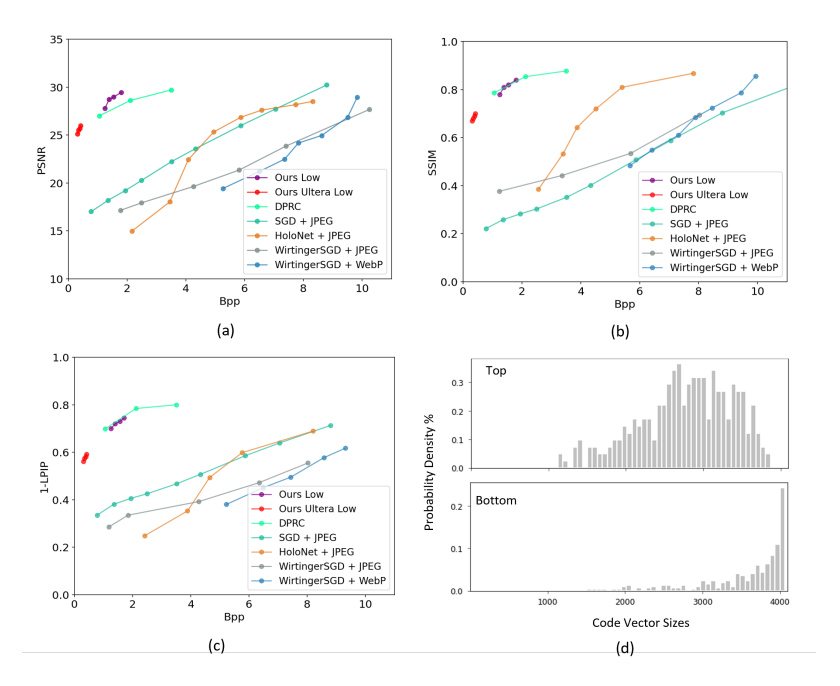


Figure 5: (a, b, c) Rate-distortion performance indicated as quality metrics vs. Bpp, (d) Code vector utilization

Compared to conventional codecs (e.g., JPEG combined with SGD, HoloNet, and WirtingerSGD and WebP combined with WirtingerSGD), our framework demonstrates a more favorable rate—distortion balance. Relative to DPRC, the best existing method, our method achieves enhancement in -33.91% BD-Rate and BD-PSNR [37] of 1.02 dB. These findings suggest that our method is well-suited for holographic image compression in bandwidth-limited scenarios, enabling efficient storage and transmission without sacrificing reconstruction quality.

3.7 Qualitative Result

Fig. 6 presents a qualitative and quantitative comparison of four image reconstruction approaches: (a) Original Amplitude, (b) SGD + JPEG, (c) DPRC, and (d) Ours. In the first row, our method (last column) successfully recovers the fine fur details of the lion—which are noticeably lost in SGD+JPEG method or have lower contrast in the DPRC method. It also achieves the highest PSNR (35.23 dB) with a competitive bit rate (1.729 Bpp).

In the second row, our method (last column) successfully recovers fine facial details—such as the wrinkles between the eyebrows with enhanced contrast—that are noticeably blurred or lost in the other methods. It also achieves the highest PSNR (31.281 dB) with a competitive bit rate (1.773 Bpp).

The third row shows a beach scene, where our reconstruction appears slightly darker than DPRC's brighter output but retains well-defined details, delivering superior fidelity (30.541 dB PSNR) at a lower bit rate (1.756 Bpp).

In the fourth row, the parrot image reconstructed by our method preserves vibrant colors and textures, achieving a similar PSNR (34.400 dB) to DPRC while requiring nearly 1 Bpp less (1.630 vs. 2.620).

Lastly, the fifth row demonstrates our method's effectiveness in reconstructing dark regions with high perceptual quality, achieving nearly the same PSNR (32.654 dB) as DPRC while using significantly fewer bits (1.740 Bpp vs. 3.120 Bpp). Overall, these results highlight the strength of our approach in preserving visual detail and quality across diverse scenes, even under tight bitrate constraints.

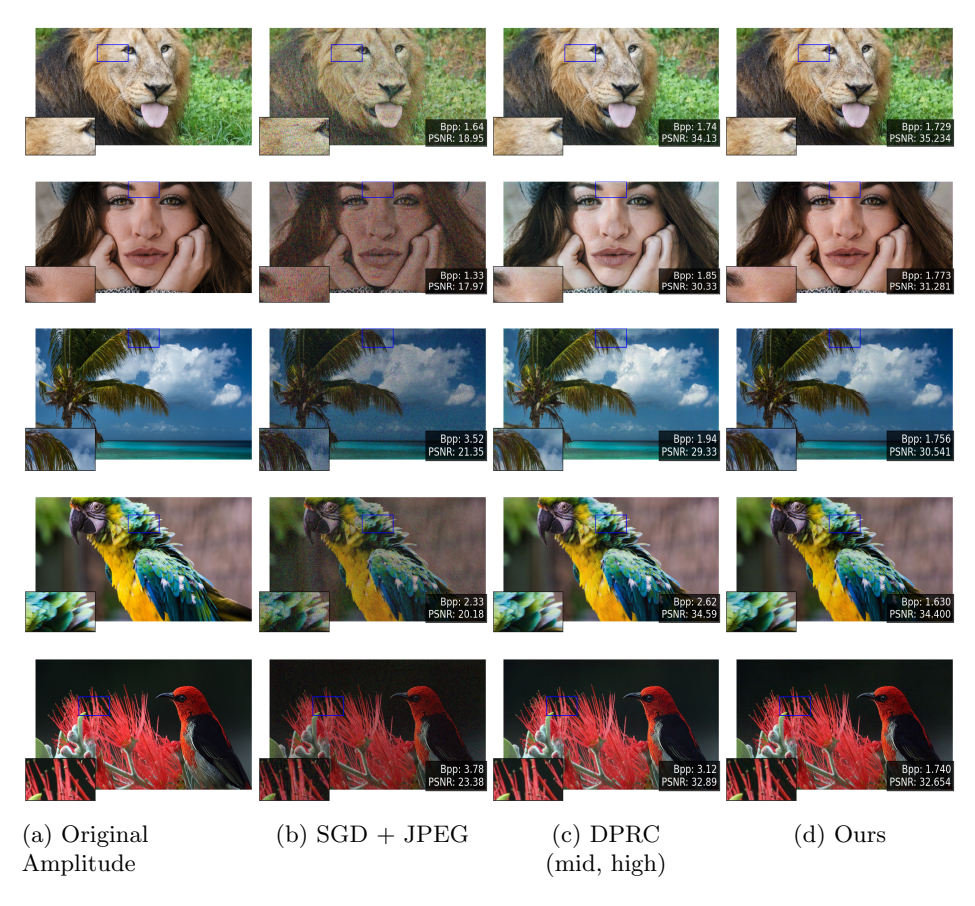


Figure 6: Numerical reconstruction. Comparison between three top methods in plot 5 on images from [32]. The first two rows show our high-quality results versus DPRC's medium-quality outputs. The last two rows compare our method with DPRC's high-quality outputs. The baseline method (SGD + JPEG) exhibits a high amount of speckle noise.

As illustrated in Fig. 7, evaluation is conducted only on the Seq2seq model's outputs that correspond to codebook sizes that are powers of two. Results are shown from both Ultra-Low and Low networks for two images of the butterfly and the statue.

4 Future work

Future extensions of this work may incorporate salient [38] or gaze-driven regions [20] to guide the reconstruction process. This would enable the network to allocate more code vectors to perceptually important areas while tolerating greater artifacts in non-salient regions, thereby improving both perceptual quality and compression efficiency. Additionally, since RGB channels share similar structural components, jointly compressing complex-valued RGB holograms is expected to be more efficient than training separate networks for each channel. In this paper, we applied our compression method to 2D holography. To extend it toward 3D holography, modalities such as RGB-D, 2.5D, and full 3D representations could be explored [39]. For example, the generator proposed in [5] could be integrated into our framework, as it is capable of producing complex-valued holograms from RGB-D inputs with continuous depth. Furthermore, approaches such as holographic stereograms or holography without Fresnel propagation (e.g., [40]) employ different data formats but could still be adapted to our framework as a combination of multiple 2D views. When working with RGB-D inputs, depth-aware propagation using models like [1] or ASM applied to masked depth maps may yield more realistic reconstructions. Moreover, techniques such as camera-in-the-loop holography [9] and calibration-aware pipelines could further help bridge the gap between simulated reconstructions and real-world holographic displays.

5 Conclusion

In this work, we presented RAVQ-HoloNet, an unsupervised, rate-adaptive framework for compressing and reconstructing complex-valued holographic data. Our approach unifies complex-valued encoding and phase generation decoder within a single network, enabling end-to-end learning from raw hologram inputs to phase-only reconstructions. By integrating a Seq2seq-based rate-adaptive vector quantization module into the VQ-HoloNet architecture, our method overcomes the limitations of fixed-rate compression, allowing multiple bitrates to be supported within a single trained model. Experimental results demonstrate that RAVQ-HoloNet achieves competitive or superior reconstruction quality compared to existing state-of-the-art methods, while operating at significantly lower Bpp rates. Both quantitative metrics (PSNR, SSIM, LPIPS) and qualitative visual comparisons confirm its ability to preserve fine details and perceptual fidelity, even under aggressive compression settings. The flexibility of our rate-adaptive design eliminates the need to store and maintain separate



Figure 7: Neumerical reconstruction. RAVQ-HoloNet with a range of Bpp containing our Low and Ultra Low networks results for the butterfly and statue in [32].

encoder—decoder pairs for each bitrate, making it highly suitable for deployment on bandwidth- and storage-constrained devices. Beyond 2D holography, our framework can be extended to 3D modalities such as RGB-D, 2.5D, and full 3D holographic representations, as well as integrated with gaze-driven or saliency-aware compression strategies. These directions, along with real-world calibration and camera-in-the-loop adaptations, form promising avenues for future research.

References

- [1] S. Choi, M. Gopakumar, Y. Peng, J. Kim, and G. Wetzstein, "Neural 3d holography: learning accurate wave propagation models for 3d holographic virtual and augmented reality displays," *ACM Transactions on Graphics* (*TOG*), vol. 40, no. 6, pp. 1–12, 2021.
- [2] A. Gilles, "Fast hologram synthesis methods for realistic 3D visualization," Theses, INSA de Rennes, Sep. 2016. [Online]. Available: https://theses.hal.science/tel-01392677
- [3] K. Matsushima and T. Shimobaba, "Band-limited angular spectrum method for numerical simulation of free-space propagation in far and near fields," *Optics Express*, vol. 17, no. 22, pp. 19662–19673, 2009.
- [4] K. Matsushima and S. Nakahara, "Extremely high-definition full-parallax computer-generated hologram created by the polygon-based method," Applied Optics, vol. 48, no. 34, pp. H54–H63, 2009.
- [5] L. Shi, B. Li, C. Kim, P. Kellnhofer, and W. Matusik, "Towards real-time photorealistic 3d holography with deep neural networks," *Nature*, vol. 591, no. 7849, pp. 234–239, 2021.
- [6] L. Shi, B. Li, and W. Matusik, "End-to-end learning of 3d phase-only holograms for holographic display," *Light: Science & Applications*, vol. 11, no. 1, p. 247, 2022.
- [7] C.-K. Hsueh and A. A. Sawchuk, "Computer-generated double-phase holograms," *Applied Optics*, vol. 17, no. 24, pp. 3874–3883, 1978.
- [8] A. Maimone, A. Georgiou, and J. S. Kollin, "Holographic near-eye displays for virtual and augmented reality," *ACM Transactions on Graphics (Tog)*, vol. 36, no. 4, pp. 1–16, 2017.
- [9] Y. Peng, S. Choi, N. Padmanaban, and G. Wetzstein, "Neural holography with camera-in-the-loop training," *ACM Transactions on Graphics (TOG)*, vol. 39, no. 6, pp. 1–14, 2020.
- [10] M. H. Eybposh *et al.*, "Deepcgh: 3d computer-generated holography using deep learning," *Opt. Express*, vol. 28, no. 18, pp. 26636–26650, Aug

- 2020. [Online]. Available: https://opg.optica.org/oe/abstract.cfm?URI=oe-28-18-26636
- [11] R. Horisaki, R. Takagi, and J. Tanida, "Deep-learning-generated holography," *Applied Optics*, vol. 57, no. 14, pp. 3859–3863, 2018.
- [12] R. Horisaki, Y. Nishizaki, K. Kitaguchi, M. Saito, and J. Tanida, "Three-dimensional deeply generated holography," *Applied Optics*, vol. 60, no. 4, pp. A323–A328, 2021.
- [13] R. W. Gerchberg and W. O. Saxton, "A practical algorithm for the determination of phase from image and diffraction plane pictures," *Optik*, vol. 35, no. 2, pp. 237–246, 1972.
- [14] B. Tobias *et al.*, "Jpeg pleno holography presents the numerical reconstruction software for holograms: an excursion in holographic views," *Applied Optics*, vol. 62, no. 10, pp. 2462–2469, 2023.
- [15] Y. Wang, P. Chakravarthula, Q. Sun, and B. Chen, "Joint neural phase retrieval and compression for energy-and computation-efficient holography on the edge," *ACM Transactions on Graphics*, vol. 41, no. 4, 2022.
- [16] M. Zhou et al., "End-to-end compression-aware computer-generated holography," Opt. Express, vol. 31, no. 26, pp. 43908–43919, Dec 2023. [Online]. Available: https://opg.optica.org/oe/abstract.cfm?URI=oe-31-26-43908
- [17] H. Ko and H. Y. Kim, "Deep learning-based compression for phase-only hologram," *IEEE Access*, vol. 9, pp. 79735–79751, 2021.
- [18] J. Ballé, D. Minnen, S. Singh, S. J. Hwang, and N. Johnston, "Variational image compression with a scale hyperprior," arXiv preprint arXiv:1802.01436, 2018.
- [19] L. Shi, R. Webb, L. Xiao, C. Kim, and C. Jang, "Neural compression for hologram images and videos," Opt. Lett., vol. 47, no. 22, pp. 6013–6016, Nov 2022. [Online]. Available: https://opg.optica.org/ol/abstract.cfm?URI=ol-47-22-6013
- [20] Z. Dong, Y. Ling, C. Xu, Y. Li, and Y. Su, "Gaze-contingent efficient hologram compression for foveated near-eye holographic displays," *Displays*, vol. 79, p. 102464, 2023.
- [21] J. Ballé, V. Laparra, and E. P. Simoncelli, "End-to-end optimized image compression," arXiv preprint arXiv:1611.01704, 2016.
- [22] J. Seo and J. Kang, "Raq-vae: Rate-adaptive vector-quantized variational autoencoder," arXiv preprint arXiv:2405.14222, 2024.
- [23] R. Ali et al., "Generating diverse high-fidelity images with vq-vae-2," Advances in Neural Information Processing Systems, vol. 32, 2019.

- [24] J. Seo, J. Lee, J. Lee, and H. Ko, "Deep compression network for enhancing numerical reconstruction quality of full-complex holograms," *Optics Express*, vol. 31, no. 15, pp. 24573–24597, 2023.
- [25] V. D. Oord *et al.*, "Neural discrete representation learning," *Advances in Neural Information Processing Systems*, vol. 30, 2017.
- [26] S. Hochreiter and J. Schmidhuber, "Long short-term memory," Neural computation, vol. 9, no. 8, pp. 1735–1780, 1997.
- [27] I. Sutskever, O. Vinyals, and Q. V. Le, "Sequence to sequence learning with neural networks," Advances in Neural Information Processing Systems (NeurIPS), 2014.
- [28] J. Rissanen and G. Langdon, "Universal modeling and coding," *IEEE Transactions on Information Theory*, vol. 27, no. 1, pp. 12–23, 1981.
- [29] J. W. Goodman, *Introduction to Fourier Optics*, 3rd ed. Greenwood Village, CO: Roberts and Company Publishers, 2005.
- [30] Z. Wang, E. Simoncelli, and A. Bovik, "Multiscale structural similarity for image quality assessment," in *The Thrity-Seventh Asilomar Conference on Signals, Systems & Computers*, 2003, vol. 2, 2003, pp. 1398–1402 Vol.2.
- [31] S. Czolbe, O. Krause, I. Cox, and C. Igel, "A loss function for generative neural networks based on watson's perceptual model," *Advances in Neural Information Processing Systems*, vol. 33, pp. 2051–2061, 2020.
- [32] E. Agustsson and R. Timofte, "Ntire 2017 challenge on single image superresolution: Dataset and study," in *Proceedings of the IEEE conference on* computer vision and pattern recognition workshops, 2017, pp. 126–135.
- [33] J. Dai, H. Qi, Y. Xiong, Y. Li, G. Zhang, H. Hu, and Y. Wei, "Deformable convolutional networks," in *Proceedings of the IEEE international conference on computer vision*, 2017, pp. 764–773.
- [34] X. Zhu, H. Hu, S. Lin, and J. Dai, "Deformable convnets v2: More deformable, better results," in *Proceedings of the IEEE/CVF conference on computer vision and pattern recognition*, 2019, pp. 9308–9316.
- [35] Z. Wang, A. C. Bovik, H. R. Sheikh, and E. P. Simoncelli, "Image quality assessment: from error visibility to structural similarity," *IEEE Transactions on Image Processing*, vol. 13, no. 4, pp. 600–612, 2004.
- [36] R. Zhang, P. Isola, A. A. Efros, E. Shechtman, and O. Wang, "The unreasonable effectiveness of deep features as a perceptual metric," in *Proceedings of the IEEE conference on computer vision and pattern recognition*, 2018, pp. 586–595.
- [37] G. Bjontegaard, "Calculation of average psnr differences between rd-curves," ITU-T SG16, Doc. VCEG-M33, 2001.

- [38] L. Wang, H. Lu, X. Ruan, and M.-H. Yang, "Deep networks for saliency detection via local estimation and global search," in *Proceedings of the IEEE conference on computer vision and pattern recognition*, 2015, pp. 3183–3192.
- [39] D. Kim, S.-W. Nam, S. Choi, J.-M. Seo, G. Wetzstein, and Y. Jeong, "Holographic parallax improves 3d perceptual realism," *ACM Trans. Graph.*, vol. 43, no. 4, Jul. 2024. [Online]. Available: https://doi.org/10.1145/3658168
- [40] E. Dashdavaa, A. Khuderchuluun, H.-Y. Wu, Y.-T. Lim, C.-W. Shin, H. Kang, S.-H. Jeon, and N. Kim, "Efficient hogel-based hologram synthesis method for holographic stereogram printing," *Applied Sciences*, vol. 10, no. 22, p. 8088, 2020.